Journal of Structural Geology 31 (2009) 802–816

Contents lists available at ScienceDirect

Journal of Structural Geology

journal homepage: www.elsevier.com/locate/jsg

The nature and origin of off-fault damage surrounding strike-slip fault zones with a wide range of displacements: A field study from the Atacama fault system, northern Chile

T.M. Mitchell*, D.R. Faulkner

Rock Deformation Laboratory, Department of Earth and Ocean Sciences, University of Liverpool, Liverpool, UK

ARTICLE INFO

Article history:
Received 15 August 2008
Received in revised form
1 May 2009
Accepted 5 May 2009
Available online 13 May 2009

Keywords:
Fault damage zone
Fault zone
Damage zone scaling
Microfracture density
Deformation
Fracture density

ABSTRACT

Damage surrounding the core of faults is represented by deformation on a range of scales from micro-fracturing of the rock matrix to macroscopic fracture networks. The spatial distribution and geometric characterization of damage at various scales can help to predict fault growth processes, subsequent mechanics, bulk hydraulic and seismological properties of a fault zone. Within the excellently exposed Atacama fault system, northern Chile, micro- and macroscale fracture densities and orientation surrounding strike-slip faults with well-constrained displacements ranging over nearly 5 orders of magnitude (~0.12 m–5000 m) have been analyzed. Faults have been studied that cut granodiorite and have been passively exhumed from 6 to 10 km depth. This allows direct comparison of the damage surrounding faults of different displacements. The faults consist of a fault core and associated damage zone. Macrofractures in the damage zone are predominantly shear fractures orientated at high angles to the faults studied. They have a reasonably well-defined exponential decrease with distance from the fault core. Microfractures are a combination of open, healed, partially healed and fluid inclusion planes (FIPs). FIPs are the earliest set of fractures and show an exponential decrease in fracture density with perpendicular distance from the fault core. Later microfractures do not show a clear relationship of microfracture density with perpendicular distance from the fault core. Damage zone widths defined by the density of FIPs scale with fault displacement but appear to reach a maximum at a few km displacement. One fault, where damage was characterized on both sides of the fault core shows no damage asymmetry. All faults appear to have a critical microfracture density at the fault core/damage zone boundary that is independent of displacement. An empirical relationship for microfracture density distribution with displacement is presented. Preferred FIP orientations have a high angle to the fault close to the fault core and become more diffuse with distance. Models that predict off-fault damage such as a migrating process zone during fault formation, wear from geometrical irregularities and dynamic rupture are all consistent with our data. We conclude it is very difficult to distinguish between them on the basis of field data alone, at least within the limits of this study.

1. Introduction

Typically, the structure of fault zones is envisaged as a fault core surrounded by a damage zone. Fault cores can occur as relatively narrow, localized slip zones containing high strain products such as gouge, breccias, cataclasites and ultracataclasites (Fig. 1a) (Aydin, 1978; Caine et al., 1996; Chester et al., 1993; Cowie and Scholz, 1992; Evans, 1990; Flinn, 1977; Kim et al., 2004; Scholz, 1987; Sibson, 1977; Wibberley and Shimamoto, 2003), or as a wider zone that contains multiple strands of fault cores (Fig. 1b) (Faulkner et al., 2003; Faulkner et al., 2008). The fault core is surrounded by a damage zone consisting of a transitional region of fractured rock, which is in turn surrounded by undeformed host rock that contains few or no deformation features associated with the faulting.

Understanding each component of fault structure is important as it gives an invaluable insight into the mechanical, hydraulic and seismological properties of faults (Ben-Zion and Sammis, 2003; Caine et al., 1996; Chester et al., 1993; Faulkner et al., 2003, 2008; Faulkner and Rutter, 2001; Wibberley and Shimamoto, 2003). The overall structure of a fault zone helps to determine the mechanical

* Corresponding author. Graduate School of Science, Hiroshima University, Department of Earth and Planetary Systems Science, Higashi-Hiroshima city 739-8526, Japan. Tel.: +81 (0)50 5806 5686; fax: +81 (0)82 424 0735.
E-mail address: tom-mitchell@hiroshima-u.ac.jp (T.M. Mitchell).

0191-8141/$ – see front matter © 2009 Elsevier Ltd. All rights reserved.
doi:10.1016/j.jsg.2009.05.002

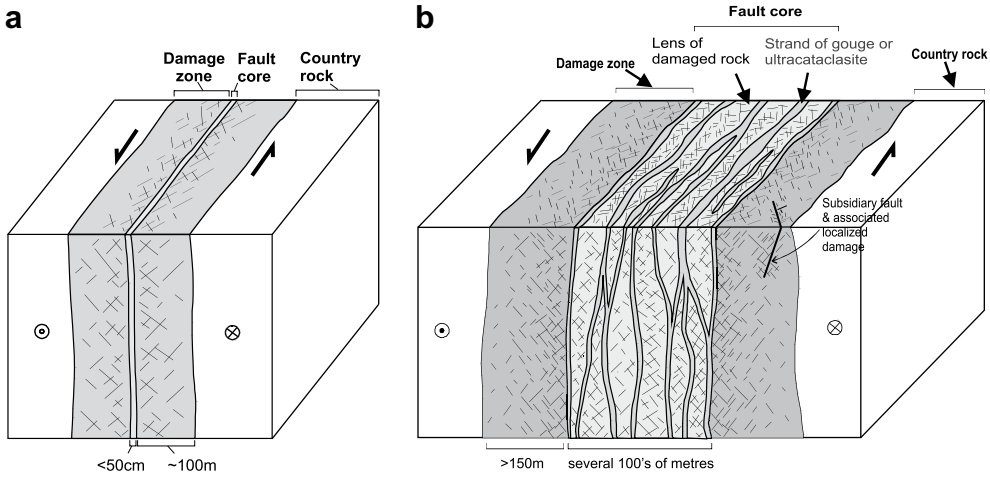

Fig. 1. Typical strike-slip fault zone structures in a quartzofeldspathic country rock (after Faulkner et al. (2003)), showing a (a) single fault core and a (b) multiple fault core, with associated damage zone.

behaviour (Biegel and Sammis, 2004; Faulkner et al., 2003). Fracturing in the damage zone may result in bi-material interfaces which may control the rupture properties of faults (e.g. Ben-Zion and Shi, 2005) in addition to affecting the fluid flow properties of the fault zone. This type of damage may also alter the stress field surrounding faults, leading to mean stress increase and stress rotations (Faulkner et al., 2006), thereby allowing high pore fluid pressure weakening of unfavourably orientated faults.

While fault core materials are typically low permeability barriers to fluid flow, the damage zone is thought to lead to hydraulic connectivity in the brittle crust, preventing fluid overpressures from developing and maintaining measured crustal stress levels in accordance with those predicted by Byerlee's law (Townend and Zoback, 2000). Co-seismic increases in permeability in the damage zone have been linked to the triggering of aftershocks as high pore fluid pressures migrate along ruptured fault zones (Miller et al., 2004). The low velocity characteristics of fractured rock present in the damage zone will dictate the P and S wave and attenuation structure of faults (Eberhart-Phillips and Michael, 1993; Rietbrock, 2001; Thurber et al., 1997). The low velocity zone will also act as a wave guide for fault zone seismic waves (Li et al., 1997).

The importance of the damage zone illustrates the need for quantitative field data on the physical dimensions, the intensity and distribution of fracture damage, and orientation of fractures within it. One of the most poorly constrained aspects of fault zone structure is the nature and origin of the damage zone (Fig. 1). Fault damage zones are represented by damage on a range of scales from microfracturing of the rock matrix to macroscopic fracture networks, and as such the empirical characterization of fracture patterns at various scales is necessary. While the physical dimensions and intensity of both microscale damage and macroscale damage within this zone as a function of distance from the fault core are fairly well documented qualitatively and quantitatively for individual faults (e.g. Anders and Wiltschko, 1994; Brock and Engelder, 1977; Faulkner et al., 2006; Scholz et al., 1993; Shipton and Cowie, 2001; Wilson et al., 2003), it is less clear how damage zones vary as a function of slip displacement and how this damage is partitioned between micro- and macrofracturing. Quantitatively comparing damage zones of faults from different regions is complicated by the fact that fault zone structure is dictated by (a) the depth of faulting (b) the protolith (c) the fault displacement and (d) the interaction with other faults and/or pre-existing structures (Faulkner et al., 2008). In particular, different studies have characterized faults that crosscut different lithologies which can have a fundamental control on fault development (Evans, 1990). Additionally, they have tended to concentrate on the structural development of relatively small faults with a correspondingly small range of displacements. The hyperarid Atacama desert in northern Chile used in this study provides excellent exposure in the Mesozoic Atacama fault system in the Coastal Cordillera, and provides an unrivalled opportunity to conduct a field study due the to well preserved fault structures that have been passively exhumed from ~6 to 9 km depth (Cembrano et al., 2005).

This study characterizes the damage surrounding faults of various slip displacements (0.12–5000 m) that cut through a single low porosity crystalline protolith. From these data it should be possible to observe any scaling relationships that might exist between slip displacement and the development of the damage zone. The applicability of various models proposed to explain the origin of off-fault damage (described in the following section) is scrutinized in light of the data presented.

2. Models of damage growth around fault zones

A key to understanding fault development is identification of the mechanical processes responsible for the origin of off-fault damage. Fracture damage surrounding fault zones may be created by various cumulative processes during or after fault formation, including Andersonian fracturing, early fault tip migration, fault tip linkage, cumulative fault wear with increasing displacement and damage imparted by dynamic rupture events (Fig. 2). These are now discussed in turn.

The first model for the production of off-fault damage is related to fault initiation (Fig. 2a). The Anderson model of faulting assumes simple, homogenous stress states in the crust and Coulomb failure behaviour and suggests that faults will form at angles of ~25–30° with respect to the maximum principal stress driving the deformation (Anderson, 1942; Scholz, 2002). It has been demonstrated experimentally and theoretically that such faults are formed through the interaction and coalescence of many tensile microcracks (Brace and Martin, 1968; Brace et al., 1966; Engelder, 1974; Healy et al., 2006; Lockner et al., 1991; Paterson and Wong, 2005; Peng and Johnson, 1972; Rutter and Hadizadeh, 1991; Scholz, 1968, 2002). These microcracks are orientated parallel to the principal compressive stress, and assuming the stress state is relatively homogeneous, microfractures surrounding a fault related to Andersonian faulting (Anderson, 1942) are expected to form at an angle of 25–30° to the

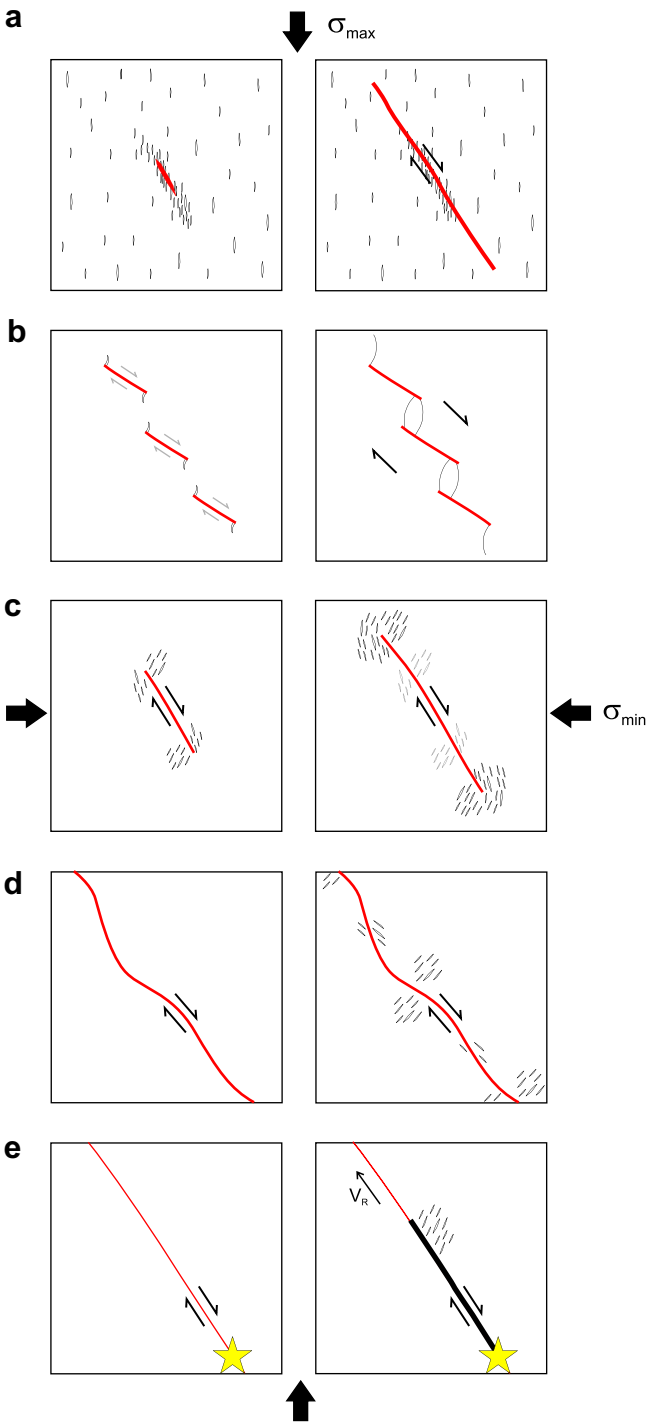

Fig. 2. Schematic diagram illustrating various models that may be responsible for creating off-fault damage, modified from Wilson et al. (2003) and Blenkinsop (2008). (a) Fault model assuming homogeneous stress, where the Andersonian model of fault formation predicts microfracture orientation at approximately 30° to the fault. Fault forms through the interaction and coalescence of many tensile microcracks. (b) Interaction of multiple fault tips model, where extension fractures formed at the tips of separate individual faults interact with each other. (c) Fault tip model for growth by tip propagation. Microfractures form in the region of the fault tip stress concentration. (d) Fault model for wear along wavy, frictional fault surfaces. (e) Off-fault damage due to the propagation of a dynamic rupture tip, with V_r being the rupture velocity that controls the form of fracturing.

fault plane (Fig. 2a). Microfractures should be diffusely distributed in the rock mass as they are a response to the large-scale remote stress, apart from the immediate vicinity of the fault plane where microfractures coalesce, and hence no variation in fracture density with distance from the shear fracture should be expected.

The second model is related to the interaction of multiple faults, where extension fractures formed at the tips of separate individual faults interact with each other. Field evidence, experiments, and theory have shown that extension fractures form around the tips of isolated fractures when loaded in shear (e.g. Blenkinsop, 2008; Engelder, 1989; Pollard and Segall, 1987; Rispoli, 1981). Such fractures are commonly referred to as wing cracks (Fig. 2b), and faulting may occur by the linkage of such flaws when two or more fault tips interact. This model would produce a damage zone of microfractures in the same orientation as the first model (Andersonian), but would be generally localized around the fault (Blenkinsop, 2008).

The third model (Fig. 2c) suggests that the bulk of the fracture damage is imparted immediately prior to fault formation in the 'process zone' surrounding the fault tip (Scholz et al., 1993; Vermilye and Scholz, 1998). This is based on non-linear and post-yield fracture mechanics models (Barenblatt, 1962; Dugdale, 1960; Scholz et al., 1993; Vermilye and Scholz, 1998). As the process zone migrates, it leaves a damage zone of microfractures in its wake. The process zone size will be determined by the magnitude of stresses surrounding the fault tip which are related to the active fault length and the remote stress, and this implies that the width of the damage zone should scale with the width of the process zone (Cowie and Scholz, 1992; Scholz et al., 1993; Scholz and Lawler, 2004). Microfracture density should decrease with distance from the fault plane, reflecting the decrease in stress concentration with distance from the fault tip. Microfracture orientations are expected to vary from high to low angles to the fault plane, dependent on whether they are in the tensile or compressive region of the fault tip respectively.

The fourth model (Fig. 2d) is related to fault wear and attributes the bulk of fault damage to the cumulative fracture damage that results from continued slip on pre-existing fault surfaces (Chester and Chester, 2000; Scholz, 1987). Fracture damage may occur due to juxtaposition of fault irregularities and consequent stress cycling (Chester and Chester, 2000; Flinn, 1977; Wilson et al., 2003). Power and Tullis (1991) and Scholz and Aviles (1986) have demonstrated that fault surfaces at all scales will show roughness, and as a result, outwardly expanding zones of damage might be expected as fault displacement accumulates, the result being that the thickness of a damage zone should scale with total fault displacement. Chester et al. (2004) highlighted that continued slip on irregular faults may ultimately overshadow the relict damage from tip propagation, which may explain why process zone models have only been successfully applied to the fabrics and fracture density distributions surrounding small and relatively immature faults. Chester and Chester (2000) showed that maximum compressive stress orientations can vary locally from parallel to perpendicular from the fault plane (e.g. Chester and Fletcher, 1997; Saucier et al., 1992), and as such microfracture orientation should vary correspondingly.

The fifth model for origin of off-fault damage (Fig. 2e) relates to earthquake rupture events (Rudnicki, 1980; Wilson et al., 2003). Generally the microfractures that are created by an earthquake rupture tip are expected to be formed in a similar orientation to the fractures formed by the migrating fault tip model, although Cowie and Scholz (1992) suggested that the region of damage may be smaller than the fault tip model predicts. Rice et al. (2005) showed that the dynamic stress field from a propagating slip pulse is dependent on rupture velocity. A supershear earthquake (where the rupture propagation exceeds the shear wave velocity) should

produce microfractures at a high angle and would only form on one side of the fault. The magnitude and extent of this damage is controlled by the stress drop of the slip event, static and dynamic friction coefficients, rupture velocity, principal pre-stress orientation and poroelastic (Skempton) coefficients. Another type of off-fault fracturing produced by dynamic rupture is 'pulverized rocks' (Dor et al., 2006a). These rocks appear to have been shattered in situ, have very fine grain size, but do not appear to have been subjected to significant shear strain. How these rocks were created is currently not fully understood. Brune et al. (1993) suggested that gouge could form explosively during the dynamic reduction of normal stress across a fault accompanying the propagation of a "wrinkle pulse" along the fault as a result of a large dynamic slip event.

3. Field study area – Atacama fault system, northern Chile

The Atacama fault zone (AFZ) is situated in the continental margin of the South American plate, beneath which oceanic lithosphere has been subducted since early Palaeozoic time (Brown et al., 1993; Mpodozis and Ramos, 1990), and is an important structure within the present day forearc of the Central Andes (Cembrano et al., 2005; Scheuber and Gonzalez, 1999). During the Mesozoic it was a major intra-arc fault system that accommodated oblique subduction between the Nazca and South American plates (Fig. 3), and it extends for ca. 1000 km between Iquique (21°S) and La Serena (30°S) (Brown et al., 1993; Cembrano et al., 2005; Scheuber and Gonzalez, 1999) within the Cordillera de la Costa of the Central Andes. The large-scale geometry of the AFS was formed during the late Jurassic and Early Cretaceous where brittle structures in excess of 60 km in length were formed by sinistral strike-slip movement (Cembrano et al., 2005). Some faults (e.g. the Caleta Coloso fault) (Fig. 3), have undergone more recent movements, although these are limited in extent, and are in response to large subduction zone earthquakes associated with the offshore trench (González et al., 2003). Some of the NS-striking master faults and subsidiary NW striking splay faults are organized into strike-slip duplexes that occur at various scales from regional to local (Cembrano et al., 2005). The faults studied in this work are all substructures of the Caleta Coloso Duplex (Fig. 3) and crosscut the Cerro Cristales pluton (González, 1990, 1996, 1999; Uribe and Niemeyer, 1984) that consists of isotropic tonalites, granodiorites and quartzo-feldspathic diorites that are classified from the variable amounts of plagioclase, quartz, orthoclase, biotite and amphibole. Fig. 4 shows examples of the granodiorite through which all of the 6 faults in this study crosscut, with an average grain size of 0.7 mm and around 30% quartz.

4. Methodology

In order to characterize the spatial variation of micro- and macroscopic damage within the fault damage zones, detailed fault transects were completed normal to the fault trace (beginning at the core/damage zone boundary) of each fault. The boundary of the damage zone and fault core was taken as the location where the cataclasite and breccia zones ceased and contacted fractured host rock. Two separate transects were completed for each fault to gain an average macrofracture density. For each transect, macroscopic fracture counts and fracture orientation measurements were completed at sampling locations every ~2–5 m. At each sampling location, an orientated sample was collected for thin-sectioning so that microfracture density and orientations could be measured under the microscope. For each transect, local lithological variations, subsidiary faults and localized cataclasite zones were noted. Structures recorded consisted of major fault planes and fractures.

The linear fracture density of macroscopic fractures was determined by counting the number of fractures intersecting along two orthogonal lines (parallel and perpendicular to the main fault trace) contained in a horizontal plane. The study was constrained to transects on only one side of the fault zones due to steep topography or the presence of alluvial cover, apart from the Blanca fault. Background macrofracture densities and orientations were measured in the area marked in Fig. 3, as this area was over 500 m away from the nearest fault and showed minimal fracture damage (pers. com. Cembrano, 2005).

To determine the microfracture density from the samples collected at each sampling locality, methods similar to those described by Anders and Wiltschko (1994) and Wilson et al. (2003) were used. Fifty evenly spaced quartz grains per sample were analyzed. Thin sections were cut perpendicular to the fault plane and parallel to the slip direction, and hence differ from the method of Anders and Wiltschko (1994) and Wilson et al. (2003) as microfractures were not measured in three orthogonal thin sections. However, this orientation provides the maximum visibility for fault-related microfractures (Engelder, 1974; Vermilye and Scholz, 1998), and we believe any differences between the sections, which were all cut in the same way, will reflect real variations in the fracture density. All visible fracture types were noted in the analysis and divided into (1) fluid inclusion planes (FIPs), (2) sealed (generally with quartz), (3) partially healed and (4) open microfractures (Fig. 7a). Quartz was selected for microfracture counts as it has little fracture anisotropy in comparison to feldspar and amphibole and hence was considered a good proxy for the total amount of microfracture damage the rock has sustained.

The microfracture density was determined by counting the number of microfractures that intersected a line of length 1.5 times the average grain diameter (Wilson et al., 2003). At each recording site consisting of randomly selected grains, the microscope stage was rotated an arbitrary amount in order to randomize the counting line orientation to minimize operator sampling bias. The total number of microfracture intersections was divided by the total counting line length to determine the average linear density of microfractures (Wilson et al., 2003). For the 3 smaller displacement faults, where damage zones were on the order of 1–10 cm, a few thin sections covered the total damage zone width, so microfracture density was measured in all quartz grains, and grains at the same distance from the fault core had their fracture densities averaged. A key aspect of this study is that grain size and mineralogy in the country rock is the same or very similar for all faults, making it easy to compare results. Microfracture orientations of FIPs were measured on selected slides for the two largest faults (Caleta Coloso and Cristales fault) using an optical microscope and universal stage (e.g. Friedman, 1969). The technique used was similar to that of Wilson et al. (2003), although no statistical weighting was applied as microfracture orientations were only determined in one thin section plane. Background microfracture densities and orientations were measured on orientated samples that were collected from the area marked in Fig. 3.

5. Results

5.1. Faults studied

Six faults which have displacements that range over nearly 5 orders of magnitude (~0.12 m–5000 m) have been studied in detail and are now described (see Table 1). For all faults, the strike-slip offset reported was measured very close to the sampling transect. The displacement profile for the faults was not measured, and while we recognize that the position of our sampling transect

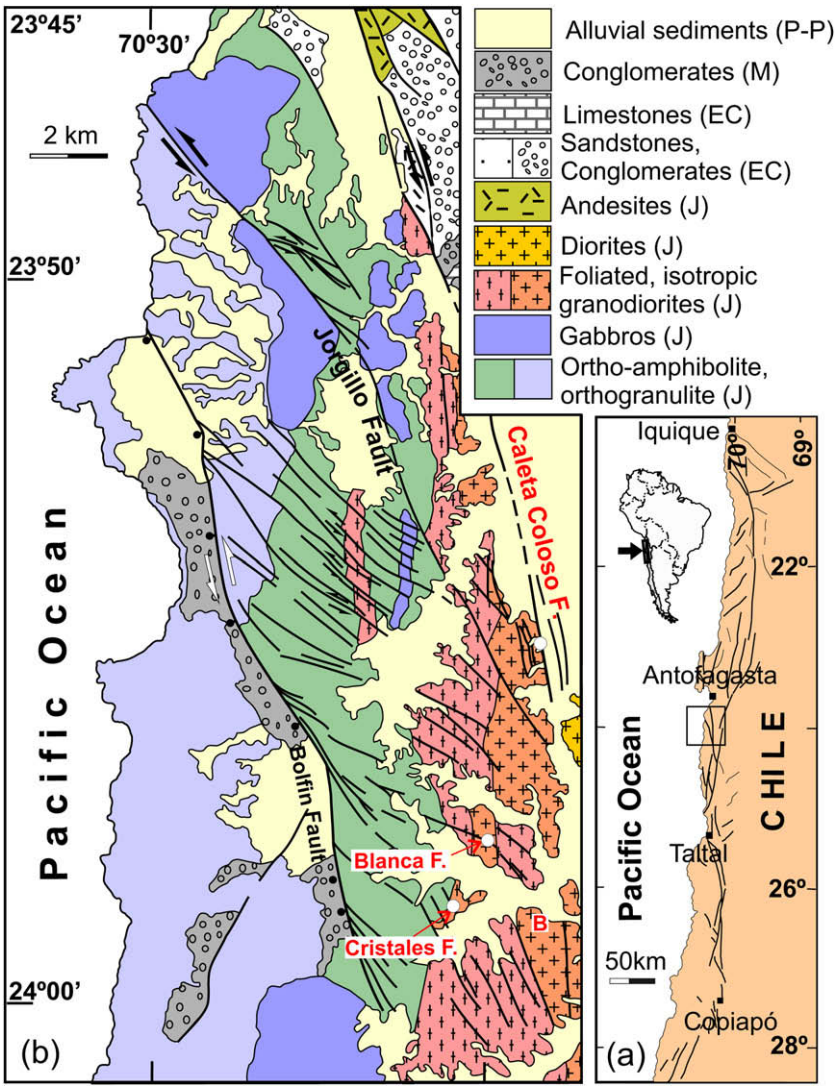

Fig. 3. Regional geological map (with inset) showing broad scale features of the Atacama fault system. (a) Atacama fault system (AFS) in the Coastal Cordillera of Northern Chile. Locations of 3 large faults are labelled in red; (b) Geology, geometry and kinematics of the sinistral strike-slip Coloso duplex, showing location of faults studied. J = Jurassic,; EC = Early Cretaceous; M = Miocene; P-P = Plio-Pliestocene. Maps simplified from (Brown et al., 1993; Cembrano et al., 2005; Scheuber & Gonzalez, 1999). Main faults and transect locations in this study are indicated, and B marks the location where background macro and microfracture counts were measured.

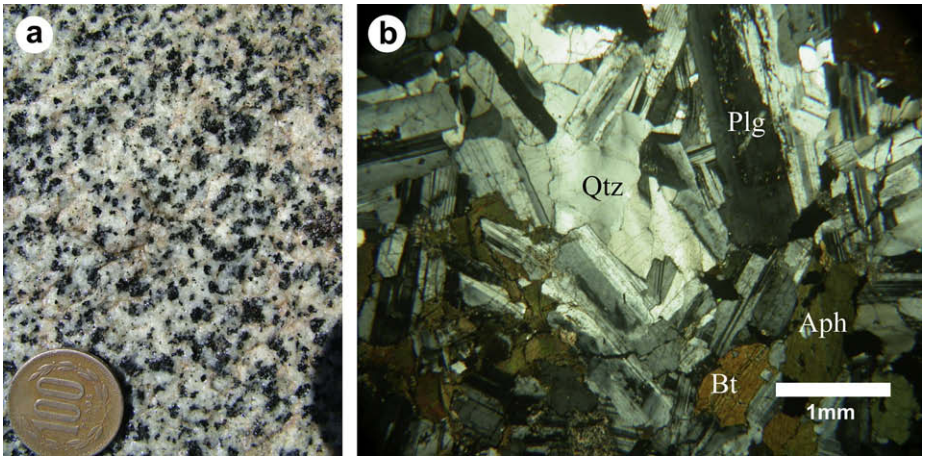

Fig. 4. (a) Field photo of intact Cerro Cristales granodiorite (b) Thin section of granodiorite in transmitted cross-polarized light. Average quartz grain size is 0.7 mm. Major phases are labelled. Qtz = quartz, Plg = plagioclase feldspar, Aph = amphibole and Bt = biotite.

relative to the displacement transect may be an important parameter, it is unconstrained in the present study.

5.1.1. Caleta Coloso fault

The Caleta Coloso fault is the largest displacement fault in this study, and has been largely passively exhumed from ~6 to 9 km depth (Cembrano et al., 2005). It lies in an NNW orientation and it extends on land at least 80 km, has a sub-vertical dip towards the west, and in plan view is slightly concave to the west (Fig. 3). Its structure is defined by a wide zone of 'multiple' fault cores (Faulkner et al., 2008) with an average thickness of ~400 m and a surrounding damage zone. The rocks within the multiple fault core are predominantly highly damaged country rock bound by discrete units of cataclasites, protocataclasites and small units of ultracataclasites (Faulkner et al., 2008) indicating multiple slip zones. Substantial and pervasive chlorite and epidote veining affect the whole fault core which gives rise to its overall distinct green colouration that clearly distinguishes the contact between core and damage zone (Fig. 5b). Slickenlines plunging at 2–8°S within the fault cores suggest predominantly strike-slip movement on an average fault plane orientation of 168 83 W (Fig. 3 h), although this can vary locally on different fault cores. The overall displacement of the Caleta Coloso fault is inferred from previous work that suggests a minimum absolute sinistral strike-slip offset of 5 km, determined by the lateral separation of a regional unconformity between the Neocomian sedimentary Caleta Coloso Formation and the underlying Jurassic volcanic and subvolcanic rocks of the La Negra Formation (Fig. 2) (Cembrano et al., 2005). There is some evidence of small cm-scale normal fault movements that postdate strike-slip displacement, as shown from topographical fault scarps in Miocene–Pliocene sediments, however these tend to be very localized around the fault core and are not widespread. Various large splay faults with unknown displacements branch off this fault and cross the transects (see Fig. 5a). The structure of this fault can be taken to be representative of faulting at depth, and can be assumed to be a crustal-scale structure by virtue of its offset.

5.1.2. Cristales fault

The Cristales fault is an excellently exposed sinistral strike-slip fault (Fig. 5c and d) that runs NNW and dips 75–80° to the west (Fig. 3h). In plan view the fault appears to extend to a minimum of 7.5 km in length. The single fault core zone is on average 4 m thick, and cuts the Cerro Cristales pluton and metadiorite Bolfin complex (Fig. 3); the fault transects in this study were within the Cerro Cristales granodiorite. The fault core is composed of several metres of cataclasites, in the centre of which is a discrete development of ultracataclasites that ranges from 10 to 14 cm thickness, with a gouge core that ranges between 20 cm and 80 cm in width. Slickenlines plunging at 11–20°S within the fault core suggest predominantly strike-slip movement (Fig. 3h), with the sense of sinistral movement determined from the P/R_1 Riedel foliation fabric within the fault gouge (Rutter et al., 1986), offset dykes and the displaced geological contacts. The magnitude of the horizontal displacement was determined by the offset contact between the Cerro Cristales Pluton and the Bolfin metadiorites (Fig. 3) at 220 m.

5.1.3. Blanca fault

The Blanca fault is well-exposed in the central part of the area in study, is orientated NNW and dips between 70 and 80°W (Fig. 5e, f and h). Nearly 2.5 km of the fault is exposed in plan view, and it is defined by a fault core composed of cataclasite that varies in width varies between 4 and 5 m, and an associated damage zone. In places with in the core, fault gouge of up to 20 cm wide can be seen. Sinistral strike-slip movement can be deduced from horizontal slickenlines, offset geological contacts and microdioritic dykes crosscutting the cataclasite core zone. Slickenlines suggest slip vectors between 6 and 14°S from the horizontal, and sinistral-normal movement determined from offset geological contacts. The magnitude of the strike-slip displacement at the sampling location is well-constrained at ~35 m, shown by displacement separation of felsic dyke very close to the studied transects.

5.1.4. Small-scale faults

The three smaller scale faults were located within the granodiorite rocks in the study region. Faults C1, FC2-8 and FC-13 are sinistral strike-slip faults, and using offset veins and dykes, displacements of 1.2 m, 2 m and 0.12 m respectively can be deduced by strike separation of planar features. Each fault has an approximate fault core thickness of 0.06, 0.03 and 0.002 m respectively, each with associated damage zones. Fig. 5g shows an example of one of these small-scale faults (FC-13), where an offset quartz vein shows the sinistral displacement (Fig. 3h). These small faults can in fact be viewed as macrofractures themselves relative to the macrofractures there were quantified within the damage zone of the three largest faults.

5.2. Macrofracturing in the damage zone

Macrofracture counts were completed on the damage zones of the three largest faults, as the smallest faults do not have sufficient displacement to accrue significant macrofracture damage. The macrofractures measured are opening and shear mode fractures or a combination of the two, and the damage zones of all 3 faults appear to contain very few filled fractures. Of the few filled fractures seen within the damage zones, the fill consisted of chlorite and epidote and there was no preferred orientation of filled fractures. Many of the fractures may be due to exhumation and/or weathering, but it is difficult to identify these from fault-related fracturing as background fracture counts show no preferred orientation.

Fig. 6 shows a graph of macrofracture density vs. perpendicular distance from the fault core for the three largest faults; Caleta Coloso, Cristales and Blanca faults. There is an exponential decrease in fracture density with perpendicular distance from the fault core for all three faults. Data are presented with a logarithmic fracture density scale, to allow a critical fracture density at zero distance from the fault to be determined from the fits to the data.

All three faults show a critical macrofracture density at 0 m of around 100 fractures per m. The locations of subsidiary faults have a clear effect on the density of macrofractures for the Caleta Coloso fault (Fig. 6), showing significantly higher fracture densities that are above the general trend, which render the data somewhat semi-quantitative. It should be noted that these points are ignored for the line of best fit (also see Wilson et al. (2003)), and are represented on the graph as the points with no border. Assuming that the point at which the macrofracture density decreases to background levels defines the outer boundary of the damaged zone i.e. damage related to the fault movement alone, then damage zone widths as

Table 1
Summary of fault data.

Fault name	Fault displacement D (m)	F_0	FIP gradients α	$1/\alpha$	Damage zone width X_{dz} (m)
Caleta Coloso	5000	17.77	0.011	91.743	149.073
Cristales	220	18.84	0.015	68.493	115.275
Blanca	35	12.64	0.070	14.368	18.450
C1	2	20.22	31.589	0.032	0.066
FC2-8	1.2	22.35	20.774	0.048	0.089
FC-13	0.13	23.03	38.962	0.026	0.060

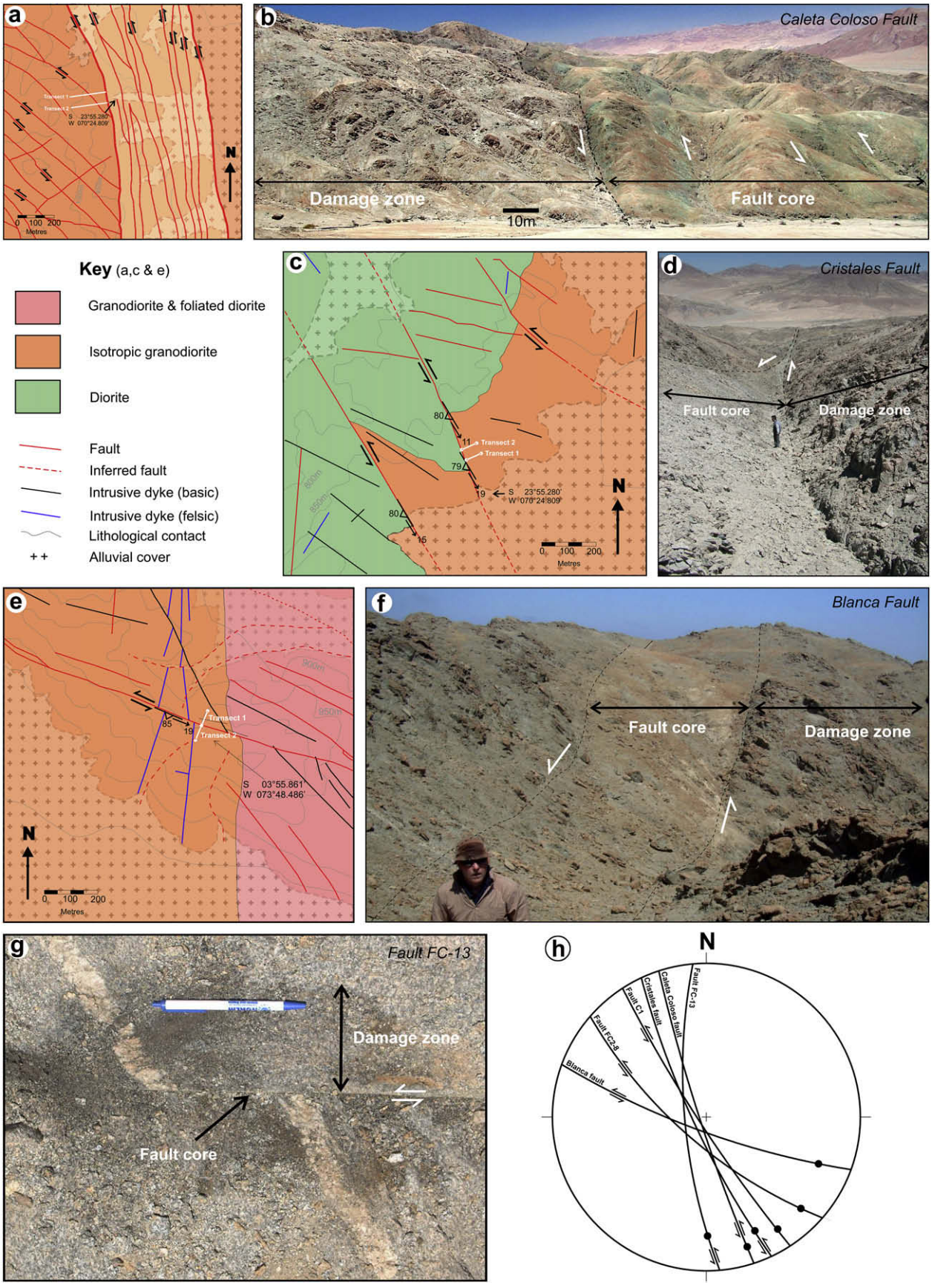

Fig. 5. Geological maps and field photos of faults studies within the Coastal Cordillera to the South of Antofagasta, Northern Chile. (a) Geological map of Caleta Coloso fault (b) View looking south along the strike of the Caleta Coloso fault (photo mirrored horizontally to match the geological map), showing the distinct fault core and damage zone. (c) Geological map of the area surrounding the Cristales fault, (d) View north along strike of the Cristales fault, (e) Geological map of the area surrounding the Blanca fault, (f) view south along the strike of the Blanca fault, (g) aerial view of the FC-13 fault/fracture. (g) Equal area projections showing the orientation of the 6 main fault planes. Slip vectors are shown as a black dot on each great circle for the corresponding fault.

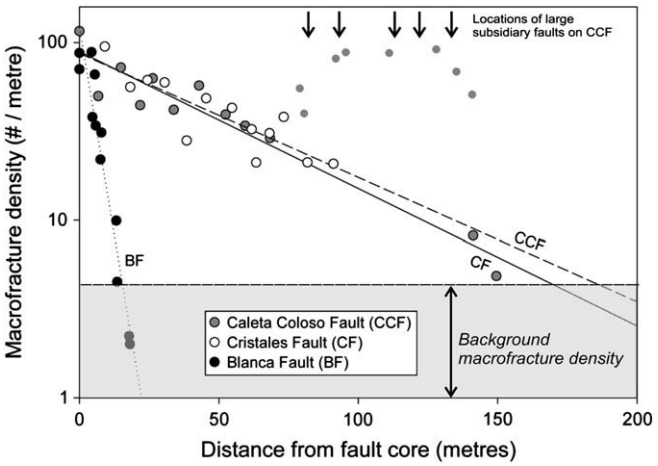

Fig. 6. Graph showing macrofracture density versus perpendicular distance from the fault core for the three largest faults. Locations of large subsidiary faults around the Caleta Coloso fault are marked with arrows. Data points where the subsidiary faults appear to have a clear effect on the density are ignored for the least square lines of best fit (represented as the points with no border).

defined by macrofractures appear to scale with fault displacement at least when comparing the smallest fault (Blanca fault) with the two larger faults (Caleta Coloso & Cristales faults). The Caleta Coloso & Cristales faults appear to have similar damage zone widths, but with the number of faults being limited to three, further analysis of faults with other displacements is required to make further comment. Background fracture counts were completed on samples from undeformed regions (Fig. 3) for both macro- and microfracture densities and orientation of background fractures. Although the subsidiary faults were not mapped in any significant detail, other studies have shown that they have similar offsets to the Blanca fault (~35 m), in which case the fall-off to background fracture densities from the fracture density peaks seen around subsidiary faults is comparable to the damage zone width of the Blanca fault.

5.3. Microfracturing in the damage zone

A qualitative analysis of the crosscutting relationships of the different microfracture types (fluid inclusion planes (FIPs), healed, partially healed and open microfractures – see Fig. 7a) suggests that these deformation features formed in a stepwise manner, with the FIPs representing the earliest period of microfracturing at the greatest depth, followed by the healed microfractures that perhaps formed at a shallower depth, then the partially healed microfractures and finally the open fractures which may be related to the faulting, but equally some of which might be stress relief microfractures related to the final exhumation of the fault to the surface.

For the Caleta Coloso fault (Fig. 7b) the FIPs show an exponential decrease in microfracture density with perpendicular distance from the fault core from just above 20 per mm to below 3 per mm with an r^2 value of 0.71. Partially open fractures show a general decrease in density with distance, although this relationship is magnified by the log scale and only shows a drop in density from 3/mm to below 1/mm with an r^2 value of 0.29. The density of open fractures and sealed fractures show no clear relationship with distance from the fault. These same relationships of the different fracture types with distance are observed for the other faults and hence we only present data for FIPs for the other faults studied. Locations of the subsidiary faults surrounding the Caleta Coloso fault have been noted on Fig. 7b, but it is difficult to say whether they have had any effect on the microfracture density. Some crosscutting relationships can be seen between the fluid inclusion planes, although it is difficult to identify clearly different generations. Preliminary cathode luminescence work (not shown here) suggests that multiple generations of fill are not seen in the FIPs.

Fig. 8a and b shows FIP microfracture density variations with perpendicular distance from the fault core for the three largest displacement faults (Fig. 8a – 5000 m, 220 m and 35 m displacement respectively) and the three smallest displacement faults (Fig. 8b – 2 m, 1.2 m and 0.13 m respectively). The FIPs show an exponential decrease in microfracture density with perpendicular distance from the fault plane for all six faults. Assuming that the decrease in microfracture density to background levels defines the outer boundary of the damaged zone, then the damage widths defined by the drop off density of FIPs appear to scale with fault displacement.

Fig. 9 shows the microfracture and macrofracture density for the Blanca Fault where data were recorded on both sides of fault core to look for any asymmetry in fracture damage. It can be seen that macro and microfracture densities are approximately symmetrical on both sides of the fault.

5.4. Microfracture orientations in the damage zone

Fig. 10 shows FIP microfracture orientations within the damage zones of the two largest faults at various distances from the fault core. In general, microfractures in the damage zone of the Caleta Coloso fault appear to be predominantly in a sinistral orientation of ~20° to the fault (counter clockwise to the slip vector). However, the plots for each distance show that at 16 m distance from the fault plane there appears to be a set of microfractures at a steeper angle (around 85°) to the fault plane that dominates over the microfractures orientated at 20°. These microfractures that are close to the fault will dominate the overall picture of microfracture orientation, as the microfracture density is much greater as the fault core is approached (Fig. 8). At 59 m the higher angle microfractures become less apparent while microfractures at 20° to the fault appear more dominant, and at distances of 107 m and 139 m the higher angle set of fractures disappear while sets of microfractures at 20° occur. It is clear that the higher angle microfractures are more common closer to the fault core. However, at 107 m there appears to be a unique set of fractures orientated at around 15° (clockwise to the slip vector) that are consistent with dextral sense of slip which dominate over the set at 20°.

For the Cristales fault microfractures at 9 m from the fault core are predominantly in an orientation of 70° to the fault plane, counter clockwise to the slip vector. This orientation dominates the microfracture fabric, also at 90 m from the fault, although some microfractures with orientations perpendicular to the fault occur. However, at 38 m there also appears to be a dominant cluster of microfractures at around 50° to the fault plane (clockwise to the slip vector), which is more consistent with a dextral sense of slip. In addition to the trends for both faults, there appears to be a background spread of microfracture orientations ranging from fault-parallel to fault-perpendicular. Microfracture orientation measurements made on the same intact samples that the background density counts were made on showed a generally diffuse microfracture fabric with no preferred orientation.

6. Discussion

In this section we discuss how the damage zone scales with fault displacement for the faults studied. We then attempt to interpret our data in terms of the current models that have been proposed for the origin of off-fault damage.

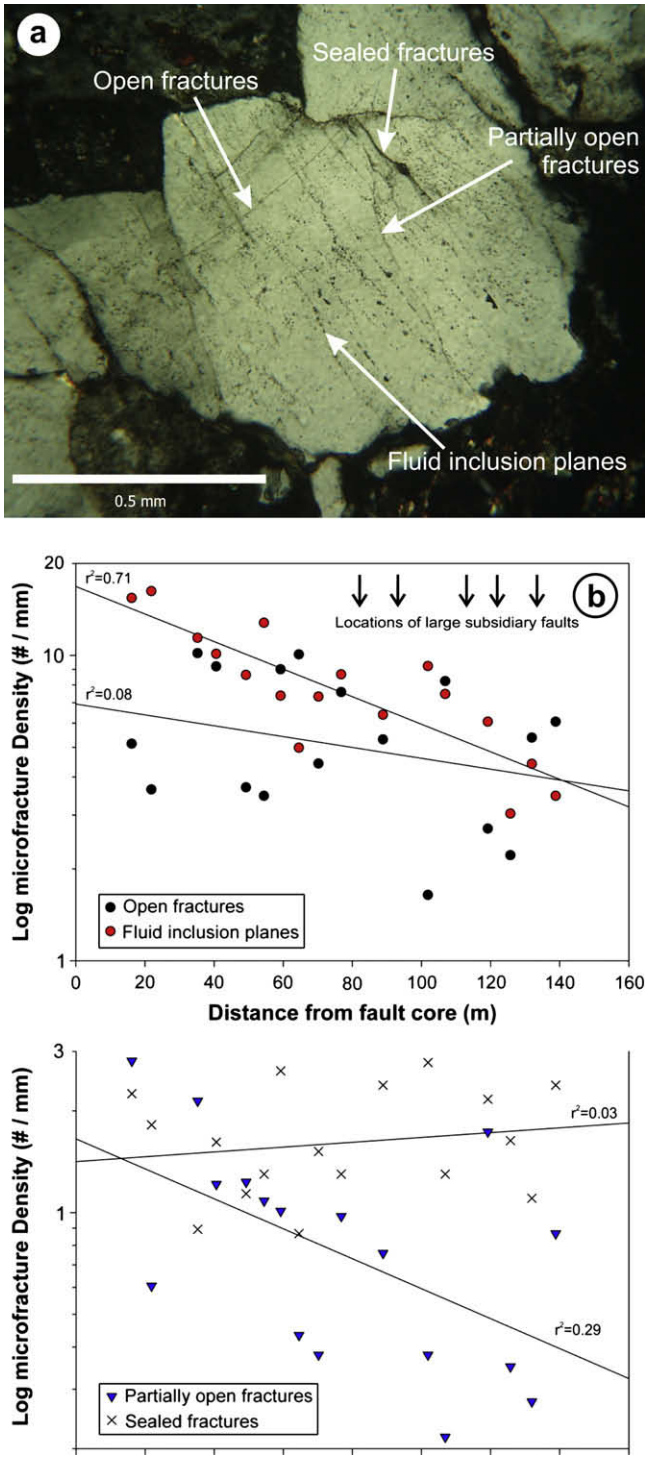

Fig. 7. (a) Optical micrograph in cross polar light showing types of microfractures; open, sealed, partially open and fluid inclusion planes. (b) Graph of microfracture density versus perpendicular distance from the fault core for open microfractures and fluid inclusions planes, and (c) partially open and sealed microfractures for the Caleta Coloso fault.

6.1. Damage zone scaling with displacement

The results from this study show that both macrofracture and microfracture densities decrease with increasing perpendicular distance from the fault core. Such results have been well documented for *individual* small faults both in experimentally deformed

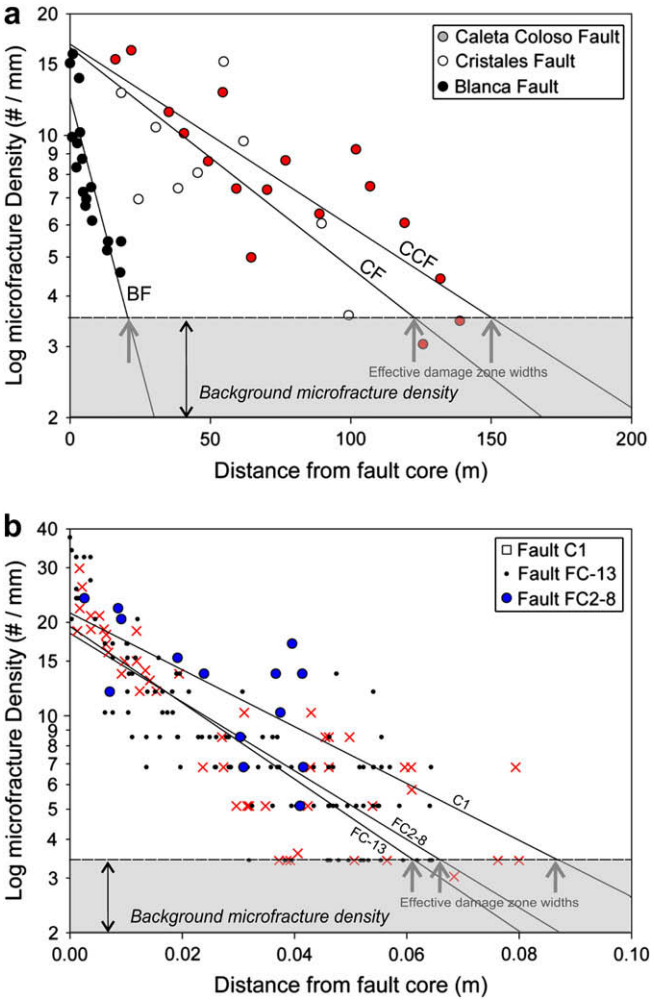

Fig. 8. Graph showing microfracture density versus perpendicular distance from the fault core for (a) the three largest faults and (b) the three smallest faults. Error in fracture density is typically ±2 microfractures/mm.

samples (Janssen et al., 2001; Moore and Lockner, 1995), faults of ranging sizes in various field studies (Anders and Wiltschko, 1994; Brock and Engelder, 1977; Scholz et al., 1993; Vermilye and Scholz, 1998; Wilson et al., 2003). Our results appear to indicate that fault damage zones vary predictably as a function of fault displacement,

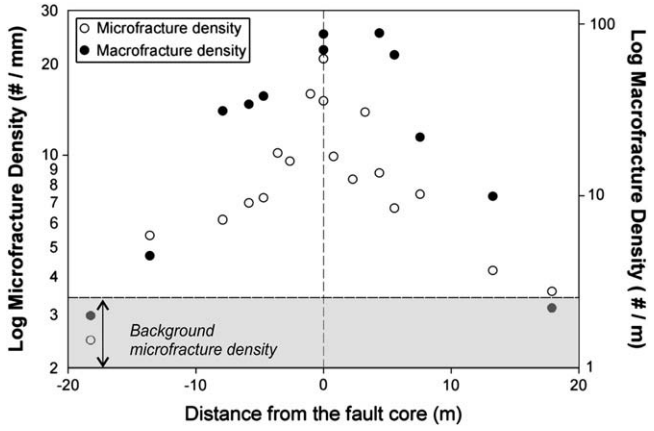

Fig. 9. Macro- and microfracture density versus perpendicular distance from the fault core for both sides of the Blanca fault.

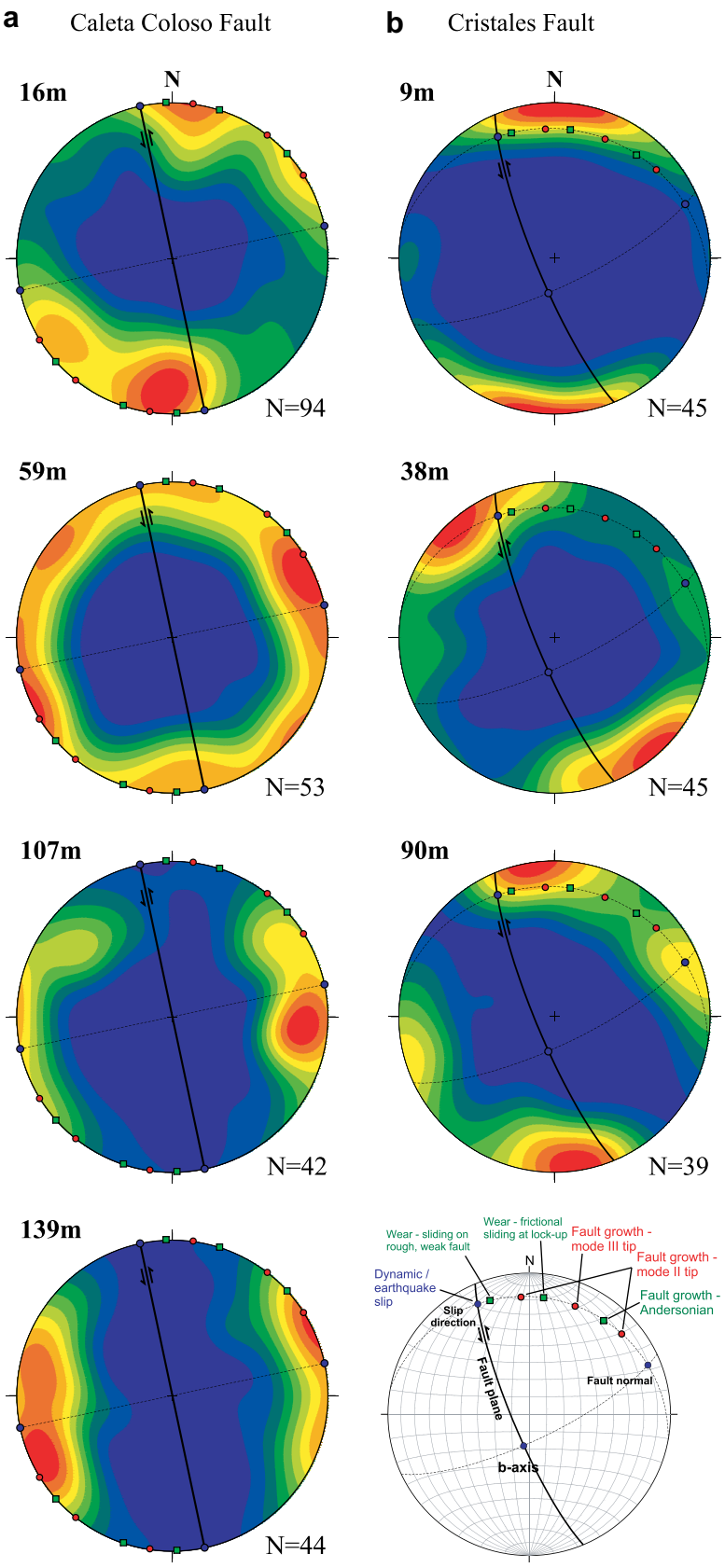

Fig. 10. Microfracture orientation versus distance from fault for (a) the Caleta Coloso fault and (b) the Cristales fault. All plots are equal area projections with contour intervals of 10 of the poles to microfracture planes. Great circles with shear sense indicators represent fault plane orientation and filled circles show the orientation of fault b-axis, normal and slip direction. Green great circles show orientation of major subsidiary faults. Bottom right Stereonet shows the expected orientation of microfractures of the various models discussed (from Wilson et al., 2003). These predictions are overlaid on all of the data for comparison.

although at higher displacements the rate of increase of the damage zone width appears to slow.

6.1.1. Macrofractures

The macrofracture densities for the three largest faults in Fig. 6 show that macrofractures decrease through the damage zone as a function of distance from the fault core. There are three key observations; 1) there is a significant difference between the damage zone widths of the two largest faults and the smaller Blanca fault; 2) there are significant increases in macrofracture density on the Caleta Coloso fault where subsidiary faults are approached/intercepted and; 3) for all 3 faults there is a common maximum macrofracture.

It is difficult to say if the damage zone width as defined by the macrofractures scales with fault displacement. The Cristales fault and Caleta Coloso fault (with displacements of 220 m and 5000 m respectively) appear to have similar damage zone widths. This may suggest that a maximum damage zone width is established above 220 m of displacement, but more data are required to explore this possibility further.

Wilson et al. (2003) showed similar increases in macrofracture density due to the proximity of subsidiary faults. It is expected that the subsidiary faults that intercept the fault transects will have their own related fracture damage with similar density-distance profiles to the faults studied in detail here; the displacements of the subsidiary faults, although not mapped, are thought to be between 20 and 50 m, so it is therefore no surprise that the subsidiary fault-related high fracture densities die off with comparable distances to the width of the damage zone of the Blanca fault ($\sim$35 m displacement).

Fig. 6 also shows that there appears to be a critical macrofracture density of around 100/m, which might be expected as there will be a certain critical level of fracturing before fracture damage is so intense that brecciation and cataclasis begin. Observations of the damage zone close to the core show very high degrees of fracturing and damage, with decreasing grain sizes due to comminution into the fault core.

Previous studies have shown that other faults have initiated on pre-existing joint planes (e.g. cooling joints), for example those described by Martel et al. (1988) for the Mount Abbott quadrangle faults in the Sierra Nevada, or the Gole Larghe fault within the Adamello batholith in the Italian Alps (Di Toro and Pennacchioni, 2005). In this study background fracture counts and orientations show no preferred orientation of joints in relatively undamaged areas of isotropic rock, and it is inferred that a majority of macrofractures are directly related to faulting. It must be noted that the background macrofracture count varied from 3/m to 30/m, and many fractures will undoubtedly be due to exhumation and associated stress release. Macrofracture orientations within the damage zone generally appear to be in a variety of shear fracture orientations typical of shear fractures surrounding strike-slip fault zones.

6.1.2. Microfractures

The occurrence of a critical microfracture density, F_0, at 0 m from the core shared by all six faults suggests that maximum microfracture density of the FIPs is independent of fault displacement. Vermilye and Scholz (1998) made similar observations where process zone microfractures show logarithmic density increases with proximity to the fault and a constant maximum density that is independent of fault length (which is proportional to fault displacement). This critical density may well be a material-dependent property, i.e. a maximum density of fracturing occurs before the rock mass loses integrity and breaks down resulting in brecciation and cataclasis. Our microfracture densities are a lot lower than in previous studies, perhaps due to the smaller proportion of quartz and preferential partitioning of fracturing within feldspars and amphiboles. As Anders and Wiltschko (1994) speculated, because the microfractures are preserved in, and the stresses are transmitted by, not just quartz but other minerals present, their proportion of the total mineralogy should affect microfracture density. Despite their study showing no relationship between microfracture density and different modal mineralogy, it still remains useful to compare data collected from different faults in lithologies that share similar modal mineralogies so as to guarantee that there is no lithological influence on the data. However, by using only microfracture counts in quartz we believe that the data are representative of the relative amount of microfracture damage that the rock surrounding all faults studied have sustained.

Fig. 8a and b shows that microfracture density with distance for all 6 faults follow the relationship:

$$F = F_0 e^{-\alpha x} \tag{1}$$

where F = fracture density (#/mm), F_0 = critical fracture density (#/mm), α = gradient, x = perpendicular distance from fault (m).

Assuming that the decrease in microfracture density to background levels defines the outer boundary of the damaged zone, then damage zone widths as defined by FIPs can be determined (Table 1). These damage zone widths appear to scale with displacement and therefore size of the fault, at least for the range of displacements of the faults analyzed in this study. Therefore, to compare between the 6 faults, the reciprocal of α of each of the fits to the data shown in Fig. 8a and b have been plotted versus displacement (Fig. 11), Fig. 11 also shows the same relationship for the damage zone width and displacement. The reciprocal of α is plotted in order to show a positive correlation. A hyperbolic fit to the data shown in Fig. 11 yields an empirical relationship of the form:

$$\frac{1}{\alpha} = \left(\frac{96.2743\,D}{119.4661 + D}\right) \tag{2}$$

where α = gradient (of density distance functions from equation (1)), D = fault displacement

By combining equations (1) and (2) an approximate empirical function can be derived for fracture density F with respect to fault displacement D, perpendicular distance to the fault x, and critical microfracture density F_0:

$$F = F_0 e^{-\left(\frac{119.4661 + D}{96.2743\,D}\right)x} \tag{3}$$

where F = fracture density, F_0 = critical fracture density, x = perpendicular distance from fault (metres), D = displacement (metres).

Thus, if the displacement of a fault is known, then the microfracture density F at distance $\times$ from the fault can be estimated. The applicability of the hyperbolic fit shown in Fig. 11 over a linear fit might be questioned. However, when extrapolating to greater fault displacements (out of the range of the faults described in his work), a linear fit will predict that the damage zone width will linearly increase with fault displacement. The hyperbolic model predicts that there is a finite limit to the damage zone width and that the rate of damage zone growth decreases with fault displacement. This is supported by the fact that the damage zone widths as defined by both microfractures and macrofracture for the two largest faults in this study with displacements of 220 m and 5000 m are similar in size relative to their displacement. Given that the Punchbowl fault (Wilson et al., 2003) with an $\sim$10 times the displacement of the Caleta Coloso fault, has a damage zone width of $\sim$150 m, even allowing for differences in protolith, the hyperbolic model might be considered to more applicable beyond the displacement range of the faults studied in this work. Preliminary comparisons of damage

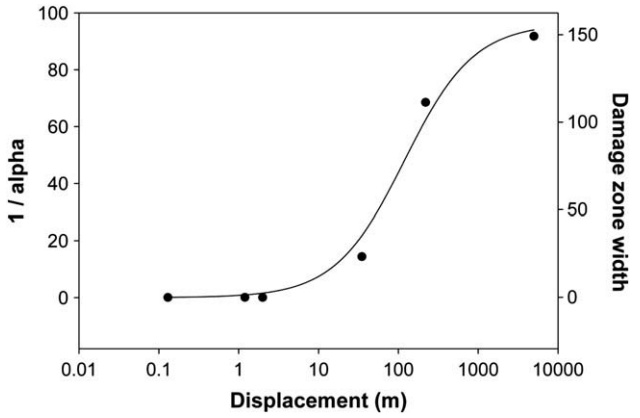

Fig. 11. Graph showing the relationship between α (gradient) and the damage zone width determined from each of the fits to the data shown in Fig. 8a and b, versus the displacement. The reciprocal of α is plotted in order to show a positive correlation.

zone widths from compiled literature data agree with this observation (Savage et al., 2008).

Anders and Wiltschko (1994) suggested that the damage zone width and critical microfracture density did not appear to vary with increasing displacement. This study agrees with Anders and Wiltschko (1994) in that there is critical microfracture density, but differs in that fracture density-distance profiles and hence damage zones widths clearly scale with fault displacement.

6.2. Models for the origin of off-fault damage

Our key observations are (1) that there are four generations of microfracture types that were operative at different times during the faulting history (2) FIPs show an exponential decrease in density with perpendicular distance from the fault plane (Fig. 8a and b) (3) a maximum FIP fracture density appears to be applicable for all the faults studied (4) damage zones as defined by FIPs scale with the fault displacement, at least in the displacement range of 0.12–220 m for the faults studied, with the largest 5000 m displacement fault showing increase in damage zone width (5) the orientation of microfractures varies widely, but broadly they have a high angle close to the fault with the exception of some localized microfracture sets.

The predicted characteristics of the five predominant models for off-fault damage are summarized in Table 2. For the microfracture orientation in all models, the normal to the average microfracture orientation (the minimum compressive stress direction) should lie in the same plane containing the slip vector of the fault studied and the normal to the fault surface (Wilson et al., 2003) (Fig. 9).

6.2.1. Andersonian model and interaction of fault tips/linkage model

The Andersonian model for damage zone development can immediately be disregarded as an oversimplification as it does not describe the data collected for FIPs (early fault damage) at all well, even though an element of this type of damage may have occurred during fault formation. Later microfracturing on the Caleta Coloso fault that does not show any logarithmic decrease with distance is consistent with Andersonian damage although the timing is not. The fault tip interaction and linkage model is also not applicable here, as larger scale field mapping show the faults to have no linkage with other faults around the sampling locations.

6.2.2. Migrating process zone model

In the migrating process zone model, the fractures produced will be the earliest set, consistent with our data for FIPs, as they are crosscut by all other microfracture types. This is also supported by the fact that FIP densities are unaffected by large subsidiary faults that crosscut the transect which appear to cause significant increases in macrofracture density, despite the thin section samples being collected close to these faults. However, it is also possible that these subsidiary faults formed at a later stage under conditions not favourable for the formation of FIPs. However, the predominant orientation of the FIPs ($\sim 70^{\circ}$) on the west side of both the Caleta Coloso fault and the Cristales fault is consistent with those expected on the tensile side of a propagating fault tip (Scholz et al., 1993), although measurements of the microfracture orientations on both sides of these faults are required to test this further.

If the FIPs do record the microfractures created from a quasi-statically migrating fault tip, then the size of the process zone (and therefore damage zone) should be controlled by the half-length of the active fracture, c, and the remotely applied stress (e.g. Lawn and Wilshaw, 1975). Cowie and Scholz (1992) suggested that the size of the zone of enhanced stress around a rupture tip is approximately 10% of the length of the slip patch. If the active fault length is the total length of the fault, then a 'dog-bone' shape to microfracture damage surrounding a fault would be predicted, as c constantly increases. However, Cowie and Shipton (1998) suggested that the active length of fault, c, that is not locked and acts to induce stress at the tip is not necessarily the same as the total fault length. The length of c in this case might reach a maximum, regardless of the total fault length. Hence the resultant size of the process zone might also reach a maximum value. Additional microfracture measurements at several locations along strike of the faults would be needed to explore this possibility.

If the fault grew as a result of a series of dynamic ruptures, then quasi-static models of fault growth may not apply. The stress fields surrounding dynamically propagating fractures wane as rupture proceeds and hence might be expected to produce decreasing process zone widths towards the fault tip from a single dynamic event (Lawn and Wilshaw, 1975). The damage pattern of multiple dynamic ruptures, if the active dynamic slip patch is approximately equal, will still result in a constant process zone size.

In this work, damage zone scaling seems to occur up to a displacement of ~ 5 km (damage zone width of ~ 150 m), although there is only a difference in damage zone width of 30 m between the 5 km and 220 m displacement faults. As previously discussed, identifying scaling beyond this 5 km displacement is not possible (see Fig. 11). Additionally, as faults become larger, the tip zones may become a lot more complicated, involving horsetail fracture geometries, fault linkage (interaction of faults with other faults) at various scales. Many fault studies have shown fault tips, fault linkages and terminations indicate that linkage zones can be on the scale of up to 400 m wide and 1 km long (Evans et al., 2000), and consist of altered and fractured rocks with numerous through-going slip surfaces.

6.2.3. Wear models

Wilson et al. (2003) showed that within the damage zone of the Punchbowl fault (San Andreas system, California) the most distinct set of microfractures were perpendicular to the slip direction of the fault and were present throughout the damage zone, implying the principal compressive stress was at right angles to the fault within the damage zone. They suggested that this is most consistent with local damage accumulation from stress cycling associated with slip on a geometrically irregular, relatively weak fault surface.

In this work, the range of microfracture orientations can equally be as well explained by the juxtaposition of geometrical irregularities as a migrating process zone. The microfracture orientation data are generally appropriate for sinistral slip, and are in orientations which can be explained by fault wear. In the Caleta Coloso fault, patterns at 16, 59, and 139 m seem to be almost entirely explicable in terms of two sets in the mode II orientations, and this explanation is

Table 2
Characteristic features of models for off-fault damage.

Model of fault damage	Microfracture timing	Microfracture orientation wrt fault	Microfracture density distribution and damage zone
Andersonian fault formation	During formation	~25–30°	Constant microfracture density with distance
Interaction of fault tip zones	During formation	~25–30°	Localized close to fault, between interacting faults
Migrating process zone	During formation	~70° on tensile side of fault tip; ~20° on compressive side of fault tip	Exponential decrease in density with distance from fault. Damage zone scales with displacement
Fault wear	Post-formation; throughout fault's history	No overall pattern predicted: fault normal to parallel	Decrease in density with distance from fault, controlled by factors such as fault roughness
Earthquake slip	Post-formation; throughout fault's history	Depends on rupture velocity (V_r) and stress drop. High V_r; high angles. Pseudotachylyte injection veins often orientated close to 90°	Decrease in density with distance from the fault. Damage zone predicted to be smaller than for migrating process zone

also compatible with the 9 and 90 m stations on the Cristales Fault. However, a key aspect of the microfracture orientation data is that in two of the patterns (107 m from the Caleta Coloso fault and 38 m from the Cristales fault), the microfracture orientations are appropriate for dextral slip that can only be explained by fault roughness effects. The scaling of the microfracture damage zone (in particular the FIPs) with fault displacement suggests that if wear were responsible, then larger irregularities would be needed to result in wider microfracture damage zone widths as fault displacement accrued.

Overprinting of earlier microfracture damage from small geometrical irregularities might result in a pattern of microfracture damage with distance that is more complex than that seen. Additionally, if overprinting does occur as displacement accumulates, then the maximum fracture density might be expected to increase. This is not seen within the FIPs, although it might be argued that the later generations of microfractures represent this progressive damage. However, the damage zone width as represented by the FIPs scales between the six faults studied, suggesting that the growth of the damage zone, via whatever process, occurred within the lifetime of the FIPs as the dominant microfracture type. The fact that the maximum fracture density does not increase between faults may also be due to the fault core increasing in width to incorporate the material with a microfracture density greater than the maximum recorded in the damage zone. Qualitatively, we do see an increase in fault core width with increasing displacement, and this process may result in a limiting value for the maximum microfracture density.

6.2.4. Dynamic rupture models

The growth of an individual earthquake rupture involves a breakdown process at the rupture tip similar to the process of fault growth (Rudnicki, 1980; Scholz et al., 1993; Swanson, 1992). As Chester et al. (2004) discussed, the structural signature from passage of a seismic rupture probably is a narrow zone or zones of concentrated shear demarcating the rupture surface within a broader zone of distributed fracturing. They suggested that the cumulative effect of numerous ruptures of large-displacement, seismic fault may be a damage zone characterized by a thickness that scales to the breakdown dimension of earthquake ruptures. They suggested that the breakdown dimension for an earthquake rupture on an existing fault is probably less than that for formation of a new fault (Cowie and Scholz, 1992). Thus, the thickness of a damage zone produced during seismic slip may be less than that produced during initial stages of fault formation and growth, but may have similar microfracture density distribution characteristics. Similar to wear models, if the damage zone is a result of multiple microfracture producing events (in this case earthquakes) then overprinting relationships might be expected, resulting in an increase in the maximum microfracture density recorded.

The orientation of microfractures related to earthquake rupture varies according to the rupture speed and the stress drop (Rice et al., 2005), although they tend to form at a relatively high angle to the fault plane. Hence the orientation of microfractures recorded in this work, with a significant component at a high angle to the Caleta Coloso and Cristales fault could be consistent with damage from earthquake rupture.

Earthquakes might be expected to produce asymmetric damage on either side of the fault, dependent on the direction of rupture propagation (e.g. Dor et al., 2006a,b). We measured the asymmetry of microfracture damage on only one of the fault studied because of constraints of exposure and time. The Blanca fault, with only ~35 m of displacement, shows fairly symmetrical fault damage (Fig. 9), and damage zone widths defined by both microfractures and macrofractures are similar in dimensions for both sides. If seismic rupture did occur, then the maximum possible magnitude would be limited by the fault's size. Hence it is not clear from our work whether asymmetric damage produced by earthquake rupture on the larger faults is a significant source of microfracture accumulation.

6.2.5. Summary

Overall, the background spread of microfracture orientations for both faults ranging fault-parallel to fault-perpendicular could be accrued from some or all of the damage models. However, some microfracture patterns seen within the damage zone can only be explained by fault wear models. The distribution of microfracture damage with distance from the fault supports the migrating process zone, wear and earthquake rupture models, although the lack of overprinting of microfractures leading to increased maximum fracture densities in close proximity to the fault is difficult to reconcile with wear and earthquake rupture models.

7. Conclusions

Within the Atacama Fault Zone, northern Chile, micro- and macroscale fracture densities and orientation surrounding strike-slip faults with well-constrained displacements ranging over 3 orders of magnitude (~0.12 m–5000 m) have been analyzed. These faults appear to share many similarities over a range of sizes; all faults are sinistral strike-slip faults that crosscut rock of granodiorite composition, and consist of a fault core and damage zone of varying widths. The faults cut granodiorite and have been passively exhumed from 6 to 10 km. This allows direct comparison of the damage surrounding faults of different displacements. All faults studied consist of a fault core and associated damage zone. Macrofractures are predominantly shear fractures orientated at high angles to the faults studied. They have a reasonably defined exponential decrease with distance from the fault core, if data points in the damage zone around the location of large subsidiary faults are

ignored. Microfractures are a combination of open, healed, partially healed and fluid inclusion planes (FIPs). FIPs are the earliest set of fractures and show a exponential decrease in fracture density with perpendicular distance from the fault core. Later microfractures do not show a clear relationship of microfracture density with perpendicular distance from the fault core. Damage zone widths, as defined by the point in the rock surrounding the fault core where FIP microfracture densities decrease to background levels, appear to scale with fault displacement for both micro- and macroscale damage, although damage zone widths appear to grow more slowly with displacements between 220 m and 5000 m. One fault, where damage was characterized on both sides of the fault core, has no damage asymmetry. All faults appear to have a critical microfracture density at the fault core/damage zone boundary that is independent of displacement. An empirical equation for microfracture density based on the evolution of displacement has been derived for these faults, allowing damage zone sizes and fracture densities to be estimated for other faults within the same material. Preferred FIP orientations have a high angle to the fault close to the fault core and become more diffuse with distance. Models that predict off-fault damage such as a migrating process zone during fault formation, wear from geometrical irregularities and dynamic rupture are all consistent with our data, although some FIP orientations seen within the damage zone can only be explained by fault roughness effects. We conclude it is very difficult to distinguish between them on the basis of field data alone, at least within the limits of this study. However, whatever the dominant processes of the generation of off-fault damage, the scaling relationships presented allow us to understand further and predict how fault zone structure and permeability evolves with displacement.

Acknowledgements

We acknowledge financial support from a Natural Environment Research Council grant (NE/C001117/1) to DRF and a University of Liverpool PhD studentship to TMM. Erik Jensen Siles, Nicolas Reyes, Dave Prior, Dave Healy and Jose Cembrano are thanked for field assistance. Tom Blenkinsop and an anonymous reviewer are thanked for their constructive reviews of the manuscript.

References

Anders, M.H., Wiltschko, D.V., 1994. Microfracturing, paleostress and the growth of faults. Journal of Structural Geology 16 (6), 795–815.
Anderson, E.M., 1942. The Dynamics of Faulting and Dyke Formation with Applications to Britain. Oliver and Boyd, Edinburgh, 191 pp.
Aydin, A., 1978. Small faults formed as deformation bands in sandstone. Pure and Applied Geophysics 116 (4–5), 913–930.
Barenblatt, G.I., 1962. The mathematical theory of equilibrium cracks in brittle fracture. Advances in Applied Mechanics 7, 25.
Ben-Zion, Y., Sammis, C.G., 2003. Characterization of fault zones. Pure and Applied Geophysics 160 (3–4), 677–715.
Ben-Zion, Y., Shi, Z.Q., 2005. Dynamic rupture on a material interface with spontaneous generation of plastic strain in the bulk. Earth and Planetary Science Letters 236 (1–2), 486–496.
Biegel, R.L., Sammis, C.G., 2004. Relating fault mechanics to fault zone structure. Advances in Geophysics 47, 65–111.
Blenkinsop, T.G., 2008. Relationships between faults, extension fractures and veins, and stress. Journal of Structural Geology 30 (5), 622–632.
Brace, W.F., Martin, R.J., 1968. A test of law of effective stress for crystalline rocks of low porosity. International Journal of Rock Mechanics and Mining Sciences 5 (5), 415.
Brace, W.F., Paulding, B.W., Scholz, C., 1966. Dilatancy in fracture of crystalline rocks. Journal of Geophysical Research 71 (16), 3939.
Brock, W.G., Engelder, T., 1977. Deformation associated with movement of muddy mountain overthrust in Buffington Window, southeastern Nevada. Geological Society of America Bulletin 88 (11), 1667–1677.
Brown, M., Diaz, F., Grocott, J., 1993. Displacement history of the Atacama fault system 25-degrees-00's–27-degrees-00's, northern Chile. Geological Society of America Bulletin 105 (9), 1165–1174.
Brune, J.N., Brown, S., Johnson, P.A., 1993. Rupture mechanism and interface separation in foam rubber models of earthquakes – a possible solution to the heat-flow paradox and the paradox of large overthrusts. Tectonophysics 218 (1–3), 59–67.
Caine, J.S., Evans, J.P., Forster, C.B., 1996. Fault zone architecture and permeability structure. Geology 24 (11), 1025–1028.
Cembrano, J., Gonzalez, G., Arancibia, G., Ahumada, I., Olivares, V., Herrera, V., 2005. Fault zone development and strain partitioning in an extensional strike-slip duplex: a case study from the Mesozoic Atacama fault system, northern Chile. Tectonophysics 400 (1–4), 105–125.
Chester, F.M., Chester, J.S., 2000. Stress and deformation along wavy frictional faults. Journal of Geophysical Research – Solid Earth 105 (B10), 23421–23430.
Chester, F.M., Chester, J.S., Kirschner, D.L., Schulz, S.E., Evans, J.P., 2004. Structure of large-displacement, strike-slip fault zones. In: Karner, G.D., Taylor, B., Driscoll, N.W., Kohlstedt, D.L. (Eds.), Rheology and Deformation in the Lithosphere at Continental Margins. Columbia Univ. Press, New York.
Chester, F.M., Evans, J.P., Biegel, R.L., 1993. Internal structure and weakening mechanisms of the San-Andreas fault. Journal of Geophysical Research – Solid Earth 98 (B1), 771–786.
Chester, J.S., Fletcher, R.C., 1997. Stress distribution and failure in anisotropic rock near a bend on a weak fault. Journal of Geophysical Research – Solid Earth 102 (B1), 693–708.
Cowie, P.A., Scholz, C.H., 1992. Physical explanation for the displacement length relationship of faults using a post-yield fracture-mechanics model. Journal of Structural Geology 14 (10), 1133–1148.
Cowie, P.A., Shipton, Z.K., 1998. Fault tip displacement gradients and process zone dimensions. Journal of Structural Geology 20 (8), 983–997.
Di Toro, G., Pennacchioni, G., 2005. Fault plane processes and mesoscopic structure of a strong-type seismogenic fault in tonalites (Adamello batholith, Southern Alps). Tectonophysics 402 (1–4), 55–80.
Dor, O., Ben-Zion, Y., Rockwell, T.K., Brune, J., 2006a. Pulverized rocks in the Mojave section of the San Andreas fault zone. Earth and Planetary Science Letters 245 (3–4), 642–654.
Dor, O., Rockwell, T.K., Ben-Zion, Y., 2006b. Geological observations of damage asymmetry in the structure of the San Jacinto, San Andreas and Punchbowl faults in southern California: a possible indicator for preferred rupture propagation direction. Pure and Applied Geophysics 163 (2–3), 301–349.
Dugdale, D.S., 1960. Yielding of steel sheets containing slits. Journal of the Mechanics and Physics of Solids 8 (2), 100–104.
Eberhart-Phillips, D., Michael, A.J., 1993. 3-Dimensional velocity structure, seismicity, and fault structure in the Parkfield region, Central California. Journal of Geophysical Research – Solid Earth 98 (B9), 15737–15758.
Engelder, J.T., 1974. Cataclasis and generation of fault gouge. Geological Society of America Bulletin 85 (10), 1515–1522.
Engelder, T., 1989. Analysis of pinnate joints in the Mount Desert Island granite – implications for postintrusion kinematics in the coastal volcanic belt, Maine. Geology 17 (6), 564–567.
Evans, J.P., 1990. Thickness displacement relationships for fault zones. Journal of Structural Geology 12 (8), 1061–1065.
Evans, J.P., Shipton, Z.K., Pachell, M.A., Lim, S.J., Robeson, K., 2000. The structure and composition of exhumed faults, and their implications for seismic processes. In: Bokelmann, G., Kovach, R.L. (Eds.), Proceedings of the Third Conference on Tectonic Problems of the San Andreas Fault System. Geological Sciences, vol. 1. Stanford University Publications, p. 14.
Faulkner, D.R., Lewis, A.C., Rutter, E.H., 2003. On the internal structure and mechanics of large strike-slip fault zones: field observations of the Carboneras fault in southeastern Spain. Tectonophysics 367 (3–4), 235–251.
Faulkner, D.R., Mitchell, T.M., Healy, D., Heap, M.J., 2006. Slip on 'weak' faults by the rotation of regional stress in the fracture damage zone. Nature 444 (7121), 922–925.
Faulkner, D.R., Mitchell, T.M., Rutter, E.H., Cembrano, J., 2008. On the structure and mechanical properties of large strike-slip faults. In: Wibberley, C.A.J., Kurz, W., Imber, J., Holdsworth, R.E., Collettini, C. (Eds.), Structure of Fault Zones: Implications for Mechanical and Fluid-flow Properties. Geological Society, London, Special Publications, vol. 299, pp. 139–150.
Faulkner, D.R., Rutter, E.H., 2001. Can the maintenance of overpressured fluids in large strike-slip fault zones explain their apparent weakness? Geology 29 (6), 503–506.
Flinn, D., 1977. Transcurrent fault and associated cataclasis in Shetland. Journal of the Geological Society of London 133, 17.
Friedman, M., 1969. Structural analysis of fractures in cores from the Saticoy Field, Ventura Co., California. American Association of Petroleum Geologists Bulletin 53, 367–389.
González, G., 1990. Patrones estructurales, modelo de ascenso emplazamiento y deformación del Plutón Cerro Cristales, Cordillera de la Costa al Sur de Antofagasta, Chile. Memoria para optar al título de Geólogo (inédita). Universidad Católica del Norte, Antofagasta, 124 pp.
González, G., 1996. Evolución tectónica de la Cordillera de la Costa de Antofagasta (Chile). In: especial referencia las deformaciones sinmagmáticas del Jurásico Cretácico Inferior. Berliner Geowissenschaftliche Abhandlungen (A), Band 181, p. 111.
González, G., 1999. Mechanismo y profundidad de emplazamiento del Plutón Cerro Cristales, Cordillera de la Costa, Antofagasta, Chile. Revista Geológica de Chile 26, 23.
González, G., Cembrano, J., Carrizo, D., Macci, A., Schneider, H., 2003. The link between forearc tectonics and Pliocene–Quaternary deformation of the Coastal Cordillera, northern Chile. Journal of South American Earth Sciences 16 (5), 321–342.

Healy, D., Jones, R.R., Holdsworth, R.E., 2006. Three-dimensional brittle shear fracturing by tensile crack interaction. Nature 439 (7072), 64–67.
Janssen, C., Wagner, F.C., Zang, A., Dresen, G., 2001. Fracture process zone in granite: a microstructural analysis. International Journal of Earth Sciences 90 (1), 46–59.
Kim, Y.S., Peacock, D.C.P., Sanderson, D.J., 2004. Fault damage zones. Journal of Structural Geology 26 (3), 503–517.
Lawn, B.R., Wilshaw, T.R., 1975. Fracture of Brittle Solids. Cambridge University Press, Cambridge.
Li, Y.G., Ellsworth, W.L., Thurber, C.H., Malin, P.E., Aki, K., 1997. Fault-zone guided waves from explosions in the San Andreas fault at Parkfield and Cienega Valley, California. Bulletin of the Seismological Society of America 87 (1), 210–221.
Lockner, D.A., Byerlee, J.D., Kuksenko, V., Ponomarev, A., Sidorin, A., 1991. Quasi-static fault growth and shear fracture energy in granite. Nature 350 (6313), 39–42.
Martel, S.J., Pollard, D.D., Segall, P., 1988. Development of simple strike-slip-fault zones, Mount Abbot quadrangle, Sierra-Nevada, California. Geological Society of America Bulletin 100 (9), 1451–1465.
Miller, S.A., Collettini, C., Chiaraluce, L., Cocco, M., Barchi, M., Kaus, B.J.P., 2004. Aftershocks driven by a high-pressure CO_2 source at depth. Nature 427 (6976), 724–727.
Moore, D.E., Lockner, D.A., 1995. The role of microcracking in shear-fracture propagation in granite. Journal of Structural Geology 17 (1), 95–114.
Mpodozis, C., Ramos, V.A., 1990. The Andes of Chile and Argentina: circum-pacific council for energy and mineral resources. Earth Science Series 11, 31.
Paterson, M.S., Wong, T.-F., 2005. Experimental Rock Deformation; the Brittle Field. Springer-Verlag, Berlin, Heidelberg, New York, 348 pp.
Peng, S., Johnson, A.M., 1972. Crack growth and faulting in cylindrical specimens of Chelmsford granite. International Journal of Rock Mechanics and Mining Sciences 9 (1), 37.
Pollard, D.D., Segall, P., 1987. Theoretical displacements and stresses near fractures in rock: with applications to faults, joints, veins, dikes, and solution surfaces. In: Atkinson, B.K. (Ed.), Fracture Mechanics of Rock. Academic Press, London, pp. 227–349.
Power, W.L., Tullis, T.E., 1991. Euclidean and fractal models for the description of rock surface-roughness. Journal of Geophysical Research – Solid Earth and Planets 96 (B1), 415–424.
Rice, J.R., Sammis, C.G., Parsons, R., 2005. Off-fault secondary failure induced by a dynamic slip pulse. Bulletin of the Seismological Society of America 95 (1), 109–134.
Rietbrock, A., 2001. P wave attenuation structure in the fault area of the 1995 Kobe earthquake. Journal of Geophysical Research – Solid Earth 106 (B3), 4141–4154.
Rispoli, R., 1981. Stress-fields about strike-slip faults inferred from stylolites and tension gashes. Tectonophysics 75 (3–4), T29–T36.
Rudnicki, J.W., 1980. Fracture-mechanics applied to the earths crust. Annual Review of Earth and Planetary Sciences 8, 489–525.
Rutter, E.H., Hadizadeh, J., 1991. On the influence of porosity on the low-temperature brittle ductile transition in siliciclastic rocks. Journal of Structural Geology 13 (5), 609.
Rutter, E.H., Maddock, R.H., Hall, S.H., White, S.H., 1986. Comparative microstructures of natural and experimentally produced clay-bearing fault gouges. Pure and Applied Geophysics 124 (1–2), 3–30.
Saucier, F., Humphreys, E., Weldon, R., 1992. Stress near geometrically complex strike-slip faults – application to the San-Andreas fault at Cajon Pass, Southern California. Journal of Geophysical Research – Solid Earth 97 (B4), 5081–5094.
Savage, H.M., Brodsky, E.E. & Johns, H. 2008. A comparison of damage zone decay around small and large faults. In: Eos Trans. AGU, vol. 89(53), Fall Meet. Suppl., Abstract T51A-1868.
Scheuber, E., Gonzalez, G., 1999. Tectonics of the Jurassic–Early Cretaceous magmatic arc of the north Chilean Coastal Cordillera (22 degrees–26 degrees S): a story of crustal deformation along a convergent plate boundary. Tectonics 18 (5), 895–910.
Scholz, C.H., 1968. Microfracturing and inelastic deformation of rock in compression. Journal of Geophysical Research 73 (4), 1417.
Scholz, C.H., 1987. Wear and gouge formation in brittle faulting. Geology 15 (6), 493–495.
Scholz, C.H., 2002. The Mechanics of Earthquakes and Faulting, second ed. Cambridge University Press, Cambridge.
Scholz, C.H., Aviles, C.A., 1986. The fractal geometry of faults and faulting. In: Das, S., Boatwright, J., Scholz, C. (Eds.), Earthquake Source Mechanics. Academic Press, New York, p. 9.
Scholz, C.H., Dawers, N.H., Yu, J.Z., Anders, M.H., 1993. Fault growth and fault scaling laws – preliminary-results. Journal of Geophysical Research – Solid Earth 98 (B12), 21951–21961.
Scholz, C.H., Lawler, T.M., 2004. Slip tapers at the tips of faults and earthquake ruptures. Geophysical Research Letters 31 (21).
Shipton, Z.K., Cowie, P.A., 2001. Damage zone and slip-surface evolution over mu m to km scales in high-porosity Navajo sandstone, Utah. Journal of Structural Geology 23 (12), 1825–1844.
Sibson, R.H., 1977. Fault rocks and fault mechanisms. Journal of the Geological Society of London 133, 22.
Swanson, M.T., 1992. Fault structure, wear mechanisms and rupture processes in pseudotachylyte generation. Tectonophysics 204, 223–242.
Thurber, C., Roecker, S., Ellsworth, W., Chen, Y., Lutter, W., Sessions, R., 1997. Two-dimensional seismic image of the San Andreas fault in the northern Gabilan range, Central California: evidence for fluids in the fault zone. Geophysical Research Letters 24 (13), 1591–1594.
Townend, J., Zoback, M.D., 2000. How faulting keeps the crust strong. Geology 28 (5), 399–402.
Uribe, F., Niemeyer, H., 1984. ranjas miloníticas en la Cordillera de la Costa de Antofagasta (Cuadrángulo de Cerro Cristales, 24°00′–24°15′S) y la distribución del basamento precámbrico. Revista Geológica de Chile 23, 4.
Vermilye, J.M., Scholz, C.H., 1998. The process zone: a microstructural view of fault growth. Journal of Geophysical Research – Solid Earth 103 (B6), 12223–12237.
Wibberley, C.A.J., Shimamoto, T., 2003. Internal structure and permeability of major strike-slip fault zones: the Median Tectonic Line in Mie Prefecture, southwest Japan. Journal of Structural Geology 25 (1), 59–78.
Wilson, J.E., Chester, J.S., Chester, F.M., 2003. Microfracture analysis of fault growth and wear processes, Punchbowl fault, San Andreas system, California. Journal of Structural Geology 25 (11), 1855–1873.